

Narrow and ultra-narrow transitions in highly charged Xe ions as probes of fifth forces

Nils-Holger Rehbehn ^{1,*} Michael K. Rosner ¹ Julian C. Berengut ^{2,1} Piet O. Schmidt ^{3,4} Thomas Pfeifer ¹ Ming Feng Gu⁵ and José R. Crespo López-Urrutia ^{1,†}

¹Max-Planck-Institut für Kernphysik, D-69117 Heidelberg, Germany

²School of Physics, University of New South Wales, Sydney, New South Wales 2052, Australia

³Physikalisch-Technische Bundesanstalt, D-38116 Braunschweig, Germany

⁴Leibniz Universität Hannover, D-30167 Hannover, Germany

⁵Space Science Laboratory, University of California, Berkeley, CA 94720, USA

(Dated: October 2, 2023)

Optical frequency metrology in atoms and ions can probe hypothetical fifth-forces between electrons and neutrons by sensing minute perturbations of the electronic wave function induced by them. A generalized King plot has been proposed to distinguish them from possible Standard Model effects arising from, e.g., finite nuclear size and electronic correlations. Additional isotopes and transitions are required for this approach. Xenon is an excellent candidate, with seven stable isotopes with zero nuclear spin, however it has no known visible ground-state transitions for high resolution spectroscopy. To address this, we have found and measured twelve magnetic-dipole lines in its highly charged ions and theoretically studied their sensitivity to fifth-forces as well as the suppression of spurious higher-order Standard Model effects. Moreover, we identified at 764.8753(16) nm a E2-type ground-state transition with 500 s excited state lifetime as a potential clock candidate further enhancing our proposed scheme.

Indirect evidence from galactic rotation, gravitational lensing and cosmological evolution suggests the existence of dark matter (DM) [1, 2]. Its constituents, by coupling to Standard Model (SM) particles, could also influence the neutrino-mass hierarchy [3] and explain open physics questions. Additional fields could cause a fifth-force coupling of electrons with neutrons, inducing small but measurable effects [4–6] in atomic systems. In an electronic transition, sensitivity to a fifth-force arises because the overlap with the nucleus changes between the ground and excited state, reflecting interactions as small as a fraction of the linewidth.

However, since the transition energies cannot be calculated accurately, isotope shift spectroscopy is employed. The classical method of the King plot (KP) uses two transitions in at least three different isotope pairs are used. Plotting the isotope shifts scaled by the nuclear-mass parameter eliminates the charge radius, typically leading to a linear behavior [7] from which atomic constants characterising atomic recoil (mass shift) and the overlap of the electronic wavefunction with the nucleus (field shift) can be derived. Optical frequency metrology has reduced uncertainties in the determination of transition energies of forbidden transitions by orders of magnitude, making KP methods far more sensitive. On top of such isotopic shifts (IS), hypothetical fifth forces would add minute perturbations causing a deviation from linearity [5, 6, 8–11]. However, unknown SM effects of higher order [6, 8] (sometimes dubbed ‘spurious’) could also induce sizable non-linearities that are hard to distinguish from those of the hypothetical forces.

A recently devised generalized King plot (GKP) [12, 13] overcomes this by using more transitions and isotope pairs to build a set of linear equations determining the higher-order effects, and even disposing of the need of exact nuclear masses (‘no-mass GKP’). Recent dedicated experiments in ytterbium measured a deviation from the King linearity [14], which has since been confirmed using other transitions [15–17]. The most likely reason for the deviation is changes in the nuclear deformation of Yb between isotopes [18], however the analysis show that a second, yet unidentified source of nonlinearity is also present. In contrast, a measurement in calcium [19], where higher-order effects are expected to be smaller, was consistent with King linearity.

To further enhance the GKP sensitivity, as many transitions and even-isotopes as possible are sought after. An ideal candidate is xenon ($Z = 54$). It has seven natural zero-nuclear-spin isotopes (124, 126, 128, 130, 132, 134, 136), and four more radio-isotopes (118, 120, 122 and 138) with lifetimes longer than minutes. Its mass reduces Doppler shifts in comparison with lighter elements, and its nuclear charge magnifies relativistic and QED effects [20], which is in itself a key field of research [21].

In this Letter, we find twelve xenon ground-state, magnetic dipole (M1) transitions in the optical region, with wavelength uncertainties in the order of 0.1 pm, and one optical electric quadrupole (E2) clock transition in charge states Xe^{9+} through Xe^{17+} . We have calculated and evaluated theoretical King plots to find which combination of transitions leads to the highest possible sensitivity to a hypothetical fifth-force between neutrons and electrons.

Highly charged ions (HCI) such as those studied here are very well suited for high-precision experiments [22], since their very low polarizability suppresses effects of external electromagnetic perturbations. Moreover, the reduced number of bound electrons reduces their theoret-

* nils.rehbehn@mpi-hd.mpg.de

† crespj@mpi-hd.mpg.de

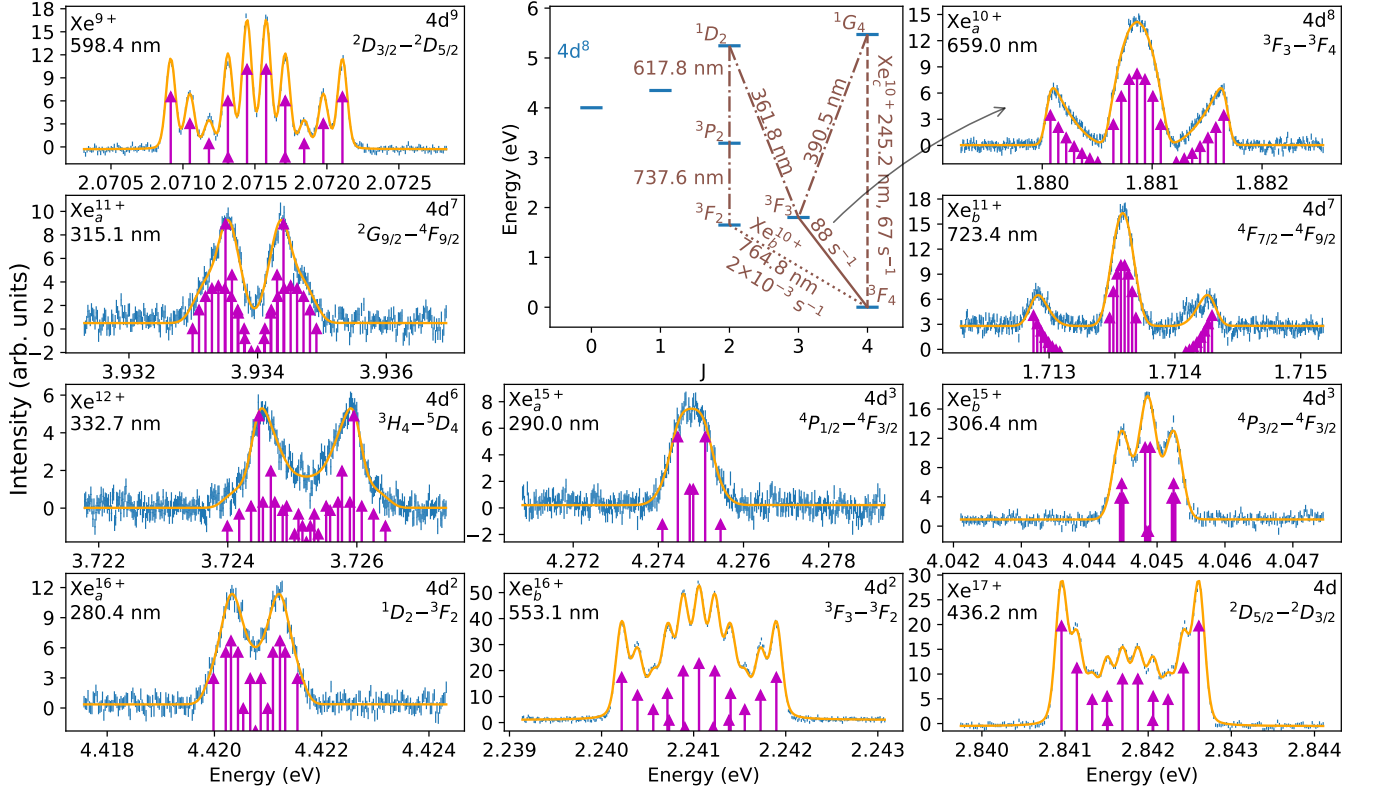


FIG. 1. Measured optical ground-state transitions of Xe^{9+} through Xe^{17+} . The Zeeman structure (arrows) was fitted based on line identification with FAC calculations. For Xe^{10+} the Grotrian diagram has been expanded. Dotted line: calculated E2 transition; dashed line: calculated M1 transition (see Supplemental Materials [URL will be inserted by publisher] for details and further Grotrian diagrams).

ical complexity. Recent experimental developments like sympathetic cooling [23], application of quantum logic spectroscopy [24] to HCI [25], and algorithmic cooling [26] have made clocks based on HCI with a sub-Hz uncertainty possible [27]. They will help extending GKP applications into beyond-the-SM (BSM) parameter regions not yet constrained by scattering experiments [28–32] and fifth-force studies [33–38].

We produced the ions of interest with an electron beam ion trap (EBIT) [40, 41], the Heidelberg EBIT (HD-EBIT) [42], from a differentially pumped atomic beam of Xe interacting with electrons at selected energies. For producing the HCI of interest Xe^{9+} through Xe^{33+} , we scanned the electron beam energy in the range 100–2500 eV in 10-eV increments. Every time the ionization potential of a given charge state is surpassed, the next higher one appears in the trap, and with it a different spectrum. In each cycle, we kept these ions trapped for 60 s, and dumped them at the end by briefly inverting the axial trapping potential set by trap electrodes. This removes impurity ions that slowly accumulate due to evaporation of barium and tungsten from the electron-gun cathode.

Electron-impact excitation populates the upper levels of the observed transitions both directly and through

casades. The electron and ion density conditions in the EBIT are such that optical magnetic-dipole transitions with Einstein coefficients higher than $\approx 10 \text{ s}^{-1}$ can be measured [43–47]. For this purpose, a set of in-vacuo lenses projects an image of the cylindrical ion cloud through a quartz vacuum window. This intermediate image is rotated by 90 degrees by a periscope and relayed by two lenses to the entrance slit of an optical spectrometer, as in Refs. [43, 44]. In the present work, we used a Czerny-Turner spectrometer with 2 m focal length [45–47] to record the wavelength range 250–800 nm, and calibrated it with hollow-cathode lamps of different elements. In its focal plane, a CCD-camera, cooled to -80°C , took several images for averaging with an exposure time of 60 minutes each. Pixels showing high signals due to cosmic muons were identified and removed from the images. Stray-light background was also subtracted. After obtaining overview spectra with a 150 grooves/mm grating, we performed measurements at higher resolution using two gratings with 1800 and 3600 grooves/mm, respectively. The results are shown in Figure 1.

For identification, we calculated for each ion the electronic structure and transition rates with the Flexible Atomic Code (FAC) [48] and AMBIT [39]. The advantage of FAC is its calculation speed, while AMBIT is used

TABLE I. Transitions in highly charged Xe ions: Measured energies, wavelengths (λ_{vac} , vacuum) and g-factors of upper and lower energy levels obtained through fitting of the Zeeman-structure with their corresponding uncertainties. Theoretical transition probabilities A_{ki} , ab-initio wavelengths and g-factors were calculated with AMBIT [39].

Ion	Transition	Observed values				AMBIT calculations				
		Energy (eV)	λ_{vac} (nm)	g_{upper}	g_{lower}	A_{ki} (s^{-1})	λ (nm)	g_{upper}	g_{lower}	Type
Xe ⁹⁺	$4d^9 \ ^2D_{3/2} - \ ^2D_{5/2}$	2.07151156(28)	598.520419(90)	0.792(2)	1.189(1)	67.5	595.4	0.8	1.2	M1
Xe _a ¹⁰⁺	$4d^8 \ ^3F_3 - \ ^3F_4$	1.8808627(14)	659.18789(56)	1.082(4)	1.238(3)	88.4	665.1	1.0833	1.2426	M1
Xe _b ¹⁰⁺	$4d^8 \ ^3F_2 - \ ^3F_4$	1.6209726(34)	764.8753(16)(Ritz)			0.002	735.6	0.9792	1.2426	E2
Xe _c ¹⁰⁺	$4d^8 \ ^1G_4 - \ ^3F_4$	5.0567231(73)	245.18684(36)(Ritz)			67.1	242.9	1.0074	1.2426	M1
Xe _a ¹¹⁺	$4d^7 \ ^2G_{9/2} - \ ^4F_{9/2}$	3.9339517(50)	315.16451(45)	1.105(37)	1.321(35)	107.7	313.3	1.0823	1.3054	M1
Xe _b ¹¹⁺	$4d^7 \ ^4F_{7/2} - \ ^4F_{9/2}$	1.71358555(87)	723.53667(37)	1.242(9)	1.306(7)	82.8	727.4	1.2276	1.3054	M1
Xe ¹²⁺	$4d^6 \ ^3H_4 - \ ^5D_4$	3.7252183(78)	332.82398(79)	1.058(32)	1.455(31)	110.8	328.6	1.0438	1.462	M1
Xe _a ¹⁵⁺	$4d^3 \ ^4P_{1/2} - \ ^4F_{3/2}$	4.2747781(74)	290.03657(50)	2.17(20)	0.78(9)	16.8	297.7	2.2137	0.47304	M1
Xe _b ¹⁵⁺	$4d^3 \ ^4P_{3/2} - \ ^4F_{3/2}$	4.0448609(24)	306.52277(20)	0.856(57)	0.799(28)	101.7	337.1	1.4357	0.47304	M1
Xe _a ¹⁶⁺	$4d^2 \ ^1D_2 - \ ^3F_2$	4.4207651(39)	280.45869(25)	1.197(11)	0.704(15)	84.4	271.3	1.2027	0.70681	M1
Xe _b ¹⁶⁺	$4d^2 \ ^3F_3 - \ ^3F_2$	2.24105833(38)	553.23949(11)	1.073(1)	0.702(2)	137.6	555.4	1.0833	0.70681	M1
Xe _c ¹⁶⁺	$4d^2 \ ^3P_1 - \ ^3F_2$	4.9243614(65)	251.77721(33)(Ritz)			10.3	244.3	1.5	0.70681	M1
Xe ¹⁷⁺	$4d \ ^2D_{5/2} - \ ^2D_{3/2}$	2.84178291(47)	436.290179(73)	1.184(2)	0.785(3)	123.7	433.8	1.2	0.8	M1

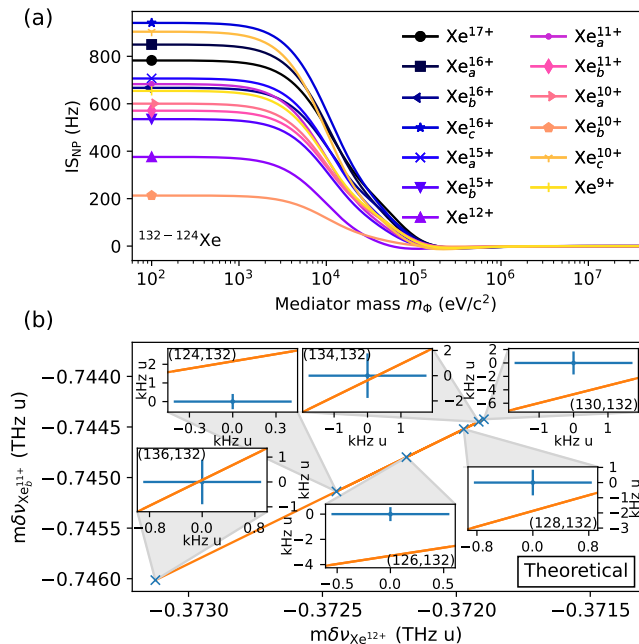


FIG. 2. (a) Isotopic shift from a hypothetical fifth-force for the forbidden ground-state transitions in Xe⁹⁺ through Xe¹⁷⁺ for a fixed coupling constant $y_e y_n = 1 \times 10^{-13}$ and varying mediator mass. (b) Theoretical King plot for the six possible Xe-isotope pairs using the Xe_b¹¹⁺, Xe¹²⁺ pair as example. We set the coupling constant to $y_e y_n = 1 \times 10^{-13}$ and the mediator mass to $m_\Phi = 1 \times 10^5 \frac{\text{eV}}{c^2}$. The error bars represent 100 mHz measurement uncertainty modified by the mass parameter μ_a .

for its more precise results. Since the 8-T field of the EBIT separates the Zeeman components to a resolvable extent, we fitted for each line its centroid, experimental linewidth, the g-factors of the upper and lower state, π

and σ amplitudes, and compare the results with theory. We corrected the identification of the 436.2 nm line in Ref. [49], from Xe¹⁸⁺ to Xe¹⁷⁺ based on the Zeeman splitting. Table I presents the key parameters of the thirteen discovered ground-state transitions. Wavelength uncertainties are the quadratic average of those from the Zeeman fits and the spectrometer dispersion. Results of AMBIT calculations are also given there: ab-initio wavelength λ , Einstein coefficient A_{ki} , and expected g-factors. Furthermore, we tabulate in the Supplemental Material [URL will be inserted by publisher] many other identified lines not involving the electronic ground-state.

A key result of our search is the identification of a ground-state clock transition of E2 electric quadrupole in Xe¹⁰⁺ from the lowest excited state. By means of Ritz-Rydberg combinations (see Supplemental Materials [URL will be inserted by publisher]), we determine for the $4d^8 \ ^3F_2 \rightarrow \ ^3F_4$ transition a vacuum wavelength of 764.8753(16) nm. We compare this with an AMBIT calculation yielding 735.6 nm and an E2 transition rate of $A_{ki} = 0.002 \text{s}^{-1}$, which is within the expected calculation uncertainty. The low transition rate suggests that this is a suitable candidate for an optical clock with a sensitivity to fifth forces that can be fully exploited due to its narrow linewidth of 0.3 mHz. We also have preliminary assignments for a few additional E2 candidates in other charge states in the Supplemental Materials [URL will be inserted by publisher], but a conclusive identification will require complementary measurements.

Following an established approach, we checked the suitability of the found ground-state transitions for GKP studies. For this, we added to the electromagnetic interaction potentials used for the FAC calculations an additional term for the hypothetical fifth-force as a Yukawa

potential [12]:

$$V_{\Phi}(r) = y_e y_n (A - Z) \frac{\hbar c}{4\pi r} \exp\left(-\frac{c}{\hbar} m_{\Phi} r\right), \quad (1)$$

where $y_e y_n$ is the coupling strength between electrons and neutrons; A the nuclear mass, Z the nuclear charge; \hbar the reduced Planck constant, and c the speed of light. The range of the force is defined by the mass parameter m_{Φ} . Using an automatized script, we performed FAC calculations varying the force range, its strength, as well as the nuclear charge radius and mass, and calculated the corresponding perturbation on the isotope-shifts.

Between two isotopes, the total isotope shift (IS) $\delta\nu_i^a = \nu_{A_{\text{ref.}}} - \nu_A$ is expressed by the following equation [12] for the transition i and the isotope pair $a = (A_{\text{ref.}}, A)$:

$$\delta\nu_i^a = K_i \mu_a + F_i \delta\langle r^2 \rangle_a + y_e y_n X_i \gamma_a. \quad (2)$$

Here, the first two terms represent the mass shift and the field shift, respectively. The former depends on the difference of the inverse of the isotope masses $\mu_a = 1/m_{A_{\text{ref.}}} - 1/m_A$, and the latter on the mean-square charge radii difference $\delta\langle r^2 \rangle_a = \langle r^2 \rangle_{A_{\text{ref.}}} - \langle r^2 \rangle_A$. The third term is caused by the fifth force, and depends on the coupling strength $y_e y_n$ between electrons and neutrons, the electronic constant $X_i = X_i(V_{\Phi})$ due to the Yukawa potential, and a factor $\gamma_a = (A_{\text{ref.}} - Z) - (A - Z)$ depending on the difference in number of neutrons. We plot the fifth-force shift versus varying mediator masses m_{Φ} in Fig. 2(a).

To study the effect of a fifth-force, we used a King plot [7], where the isotope shift in Eq. 2 is divided by the mass parameter μ_a , which then yields a common nuclear parameter $\delta\langle r^2 \rangle_a / \mu_a$ in the SM part. Between two modified transitions, the SM parts lead to a linear behavior, but a fifth-force would break it. For the six Xe-isotope pairs this is shown as theoretical prediction in Fig. 2(b). The mediator mass $m_{\Phi} = 1 \times 10^5 \frac{\text{eV}}{c^2}$ and the coupling parameter $y_e y_n = 10^{-13}$ are fixed at arbitrary, but theoretically possible values [6]. Mass uncertainties are neglected. The fifth-force shift in Fig. 2(a) is on the order of hundreds of Hz, but only a small fraction remains as a non-linearity due to the alignment of the SM linearity with the fifth-force contributions [6].

Although each pairing of transitions experiences a different non-linearity, similar fine-structure transitions share common-mode shifts, reducing the total sensitivity as in Refs. [13, 47]. Following these works, we quantified non-linearities in the King plot with the area NL spanned by the isotope pairs. Error propagation of the assumed measurement uncertainty on the isotope-shifts yielded its uncertainty ΔNL . With this, we defined the resolution R as $R = \text{NL}/\Delta\text{NL}$. A value $R = 1$ sets the lower bound of the coupling parameter $y_e y_n$ that can be resolved, as shown for given transition pairs in Fig. 3.

We assume a frequency uncertainty of $\Delta\nu = 100$ mHz as recently achieved [25, 27] and discussed in Ref. [47]. Dashed lines in Fig. 3 depict King plots neglecting mass

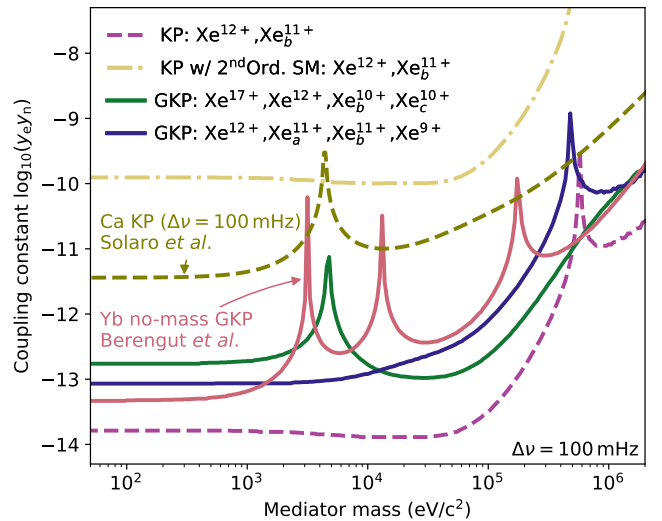


FIG. 3. Sensitivity limit for $y_e y_n$ for selected transition pairs with assumed frequency uncertainty of 100 mHz. Dashed lines: Classical King plot (KP) neglecting mass uncertainty. Calcium King plot from Solaro *et al.* [19] with 100 mHz uncertainty included for comparison. Dash-dotted line: Inclusion of a second-order field shift of 1 kHz and mass uncertainty. Solid lines: Predicted no-mass GKP for Yb [13] and for the present Xe, using four transitions.

uncertainty and higher-order SM effects. Inclusion of the former in one of these pairs, e.g., Xe^{12+} , Xe_b^{11+} , for isotopes 130 to 136 (relative mass uncertainties $\approx 10^{-10}$) and 124 to 128 (between 10^{-8} and 10^{-7}) [50] diminishes sensitivity by three orders of magnitude. Another order of magnitude is lost if nuclear deformation causes a second-order field shift of 1 kHz (dash-dotted line) [18, 51] estimated by evaluating calculated higher-order shifts in other elements [8]. We can overcome these losses with a no-mass generalized King plot [13] (shown as solid line) by adding more transitions to expand the King plot into a higher dimension. This restores the sensitivity by three orders of magnitude, as shown in Fig. 3 and brings it to the level of the ytterbium GKP with an assumed frequency uncertainty of 100 mHz from Ref. [13]. A different xenon pairing would improve the sensitivity around 10^5 eV. Full sensitivity is not recovered due to the error propagation of the four transitions needed. Note that either a reduction of the ν -uncertainty down to 5 mHz, as already achieved by optical clocks [52], or a separate, sufficiently accurate mass measurement would lead to better sensitivity.

If more higher-order SM contributions are expected, more transitions can be used to suppress their spurious effects. The seven stable even isotopes of Xe can tackle up to three such ‘spurions’ by expanding the KP into five dimensions. With thirteen ground-state transitions, one can use various pairings to optimize sensitivity to NP. By contrast, other candidates such as calcium or ytterbium only have enough even isotopes to suppress one ‘spurion’.

In the future, we plan to extend our search towards the EUV region to include ground-state transitions of even higher-charged xenon ions. This increases the number of transitions and their GKP sensitivity, as electronic wave functions with stronger overlap with the nucleus are involved. Currently emerging and continuously developing EUV frequency combs [53–56] should in the future allow frequency metrology on HCI in this spectral regime. Moreover, the presently assumed uncertainty of 100 mHz is due to that of the SI second reference, which is a Cs transition [57, 58]. By performing direct frequency comparisons with optical clocks [59–61], or by measuring the isotope shift of simultaneously trapped ions [62], one could enhance sensitivity even by a few orders of magnitude.

In summary, we found and identified thirteen optical ground-state transitions in highly charged xenon ions, theoretically analyzed them, and evaluated pairs with high sensitivity to Yukawa-type fifth-forces. Such pairings overcome limitations caused by both known and unknown SM effects by enabling the method of no-mass generalized King plots. We found for xenon a sensitivity already comparable to ytterbium, but with the clear advantage of its more numerous even isotopes and reduced nuclear deformation for future frequency metrology with sub-Hz uncertainty. Moreover, we identified a ground-state ultra-narrow clock (E2) transition with 0.3 mHz linewidth complementing the other twelve M1

lines. The analysis of this set of transitions can also be used to conduct further tests of nuclear deformation [63].

ACKNOWLEDGEMENTS

Financial support was provided by the Max-Planck-Gesellschaft. We acknowledge support from the Max Planck-Riken-PTB Center for Time, Constants and Fundamental Symmetries, the collaborative research center “SFB 1225 (ISOQUANT)” and the Deutsche Forschungsgemeinschaft (DFG, German Research Foundation) under Germany’s Excellence Strategy – EXC-2123 QuantumFrontiers – 390837967. JCB was supported in this work by the Alexander von Humboldt Foundation and the Australian Research Council (DP190100974). This work has been funded by the “European Metrology Program for Innovation and Research” (EMPIR) project 20FUN01 TSCAC. This project has received funding from the EMPIR programme co-financed by the participating states and from the European Union’s Horizon 2020 research and innovation programme. This project has received funding from the European Research Council (ERC) under the European Union’s Horizon 2020 research and innovation programme (grant agreement No 101019987).

-
- [1] G. Bertone, D. Hooper, and J. Silk, Particle dark matter: evidence, candidates and constraints, *Physics Reports* **405**, 279 (2005).
 - [2] G. Bertone and D. Hooper, History of dark matter, *Rev. Mod. Phys.* **90**, 045002 (2018).
 - [3] J. Alvey and M. Fairbairn, Linking scalar dark matter and neutrino masses with icecube 170922a, *Journal of Cosmology and Astroparticle Physics* **2019** (07), 041.
 - [4] M. S. Safronova, D. Budker, D. DeMille, D. F. J. Kimball, A. Derevianko, and C. W. Clark, Search for new physics with atoms and molecules, *Rev. Mod. Phys.* **90**, 025008 (2018).
 - [5] C. Frugiuele, E. Fuchs, G. Perez, and M. Schlaffer, Constraining new physics models with isotope shift spectroscopy, *Phys. Rev. D* **96**, 015011 (2017).
 - [6] J. C. Berengut, D. Budker, C. Delaunay, V. V. Flambaum, C. Frugiuele, E. Fuchs, C. Grojean, R. Harnik, R. Ozeri, G. Perez, and Y. Soreq, Probing new long-range interactions by isotope shift spectroscopy, *Phys. Rev. Lett.* **120**, 091801 (2018).
 - [7] W. H. King, Comments on the article “peculiarities of the isotope shift in the samarium spectrum”, *J. Opt. Soc. Am.* **53**, 638 (1963).
 - [8] V. V. Flambaum, A. J. Geddes, and A. V. Viatkina, Isotope shift, nonlinearity of king plots, and the search for new particles, *Phys. Rev. A* **97**, 032510 (2018).
 - [9] S. Fichet, Quantum forces from dark matter and where to find them, *Phys. Rev. Lett.* **120**, 131801 (2018).
 - [10] G. W. F. Drake, H. S. Dhindsa, and V. J. Marton, King and second-king plots with optimized sensitivity for lithium ions, *Phys. Rev. A* **104**, L060801 (2021).
 - [11] H. S. Dhindsa, V. J. Marton, and G. W. F. Drake, Search for light bosons with king and second-king plots optimized for lithium ions, *Physics of Particles and Nuclei* **53**, 800 (2022).
 - [12] K. Mikami, M. Tanaka, and Y. Yamamoto, Probing new intra-atomic force with isotope shifts, *The European Physical Journal C* **77**, 896 (2017).
 - [13] J. C. Berengut, C. Delaunay, A. Geddes, and Y. Soreq, Generalized king linearity and new physics searches with isotope shifts, *Phys. Rev. Research* **2**, 043444 (2020).
 - [14] I. Counts, J. Hur, D. P. L. Aude Craik, H. Jeon, C. Leung, J. C. Berengut, A. Geddes, A. Kawasaki, W. Jhe, and V. Vuletić, Evidence for nonlinear isotope shift in Yb⁺ search for new boson, *Phys. Rev. Lett.* **125**, 123002 (2020).
 - [15] N. L. Figueroa, J. C. Berengut, V. A. Dzuba, V. V. Flambaum, D. Budker, and D. Antypas, Precision determination of isotope shifts in ytterbium and implications for new physics, *Phys. Rev. Lett.* **128**, 073001 (2022).
 - [16] K. Ono, Y. Saito, T. Ishiyama, T. Higomoto, T. Takano, Y. Takasu, Y. Yamamoto, M. Tanaka, and Y. Takahashi, Observation of nonlinearity of generalized king plot in the search for new boson, *Phys. Rev. X* **12**, 021033 (2022).
 - [17] J. Hur, D. P. L. Aude Craik, I. Counts, E. Knyazev, L. Caldwell, C. Leung, S. Pandey, J. C. Berengut, A. Geddes, W. Nazarewicz, P.-G. Reinhard,

- A. Kawasaki, H. Jeon, W. Jhe, and V. Vuletić, Evidence of two-source king plot nonlinearity in spectroscopic search for new boson, *Phys. Rev. Lett.* **128**, 163201 (2022).
- [18] S. O. Allehabi, V. A. Dzuba, V. V. Flambaum, and A. V. Afanasjev, Nuclear deformation as a source of the nonlinearity of the king plot in the Yb^+ ion, *Phys. Rev. A* **103**, L030801 (2021).
- [19] C. Solaro, S. Meyer, K. Fisher, J. C. Berengut, E. Fuchs, and M. Drewsen, Improved isotope-shift-based bounds on bosons beyond the standard model through measurements of the $^2\text{D}_{3/2} - ^2\text{D}_{5/2}$ interval in Ca^+ , *Phys. Rev. Lett.* **125**, 123003 (2020).
- [20] V. M. Shabaev, A. I. Bondarev, D. A. Glazov, M. Y. Kaygorodov, Y. S. Kozhedub, I. A. Maltsev, A. V. Malyshev, R. V. Popov, I. I. Tupitsyn, and N. A. Zubova, Stringent tests of QED using highly charged ions, *Hyperfine Interactions* **239**, 60 (2018).
- [21] P. Indelicato, QED tests with highly charged ions, *Journal of Physics B: Atomic, Molecular and Optical Physics* **52**, 232001 (2019).
- [22] M. G. Kozlov, M. S. Safronova, J. R. Crespo López-Urrutia, and P. O. Schmidt, Highly charged ions: Optical clocks and applications in fundamental physics, *Rev. Mod. Phys.* **90**, 045005 (2018).
- [23] L. Schmöger, O. O. Versolato, M. Schwarz, M. Kohlen, A. Windberger, B. Piest, S. Feuchtenbeiner, J. Pedregosa-Gutierrez, T. Leopold, P. Micke, A. K. Hansen, T. M. Baumann, M. Drewsen, J. Ullrich, P. O. Schmidt, and J. R. C. López-Urrutia, Coulomb crystallization of highly charged ions, *Science* **347**, 1233 (2015).
- [24] P. O. Schmidt, T. Rosenband, C. Langer, W. M. Itano, J. C. Bergquist, and D. J. Wineland, Spectroscopy using quantum logic, *Science* **309**, 749 (2005).
- [25] P. Micke, T. Leopold, S. A. King, E. Benkler, L. J. Spieß, L. Schmöger, M. Schwarz, J. R. Crespo López-Urrutia, and P. O. Schmidt, Coherent laser spectroscopy of highly charged ions using quantum logic, *Nature* **578**, 60 (2020).
- [26] S. A. King, L. J. Spieß, P. Micke, A. Wilzewski, T. Leopold, J. R. Crespo López-Urrutia, and P. O. Schmidt, Algorithmic Ground-State Cooling of Weakly Coupled Oscillators Using Quantum Logic, *Phys. Rev. X* **11**, 041049 (2021).
- [27] S. A. King, L. J. Spieß, P. Micke, A. Wilzewski, T. Leopold, E. Benkler, R. Lange, N. Huntemann, A. Surzhykov, V. A. Yerokhin, J. R. Crespo López-Urrutia, and P. O. Schmidt, An optical atomic clock based on a highly charged ion, *Nature* **611**, 43 (2022).
- [28] R. Barbieri and T. Ericson, Evidence against the existence of a low mass scalar boson from neutron-nucleus scattering, *Physics Letters B* **57**, 270 (1975).
- [29] H. Leeb and J. Schmiedmayer, Constraint on hypothetical light interacting bosons from low-energy neutron experiments, *Phys. Rev. Lett.* **68**, 1472 (1992).
- [30] V. V. Nesvizhevsky, G. Pignol, and K. V. Protasov, Neutron scattering and extra-short-range interactions, *Phys. Rev. D* **77**, 034020 (2008).
- [31] Y. N. Pokotilovski, Constraints on new interactions from neutron scattering experiments, *Physics of Atomic Nuclei* **69**, 924 (2006).
- [32] S. L. Adler, R. F. Dashen, and S. B. Treiman, Comments on proposed explanations for the muonic-atom x-ray discrepancy, *Phys. Rev. D* **10**, 3728 (1974).
- [33] M. Bordag, U. Mohideen, and V. Mostepanenko, New developments in the casimir effect, *Physics Reports* **353**, 1 (2001).
- [34] M. Bordag, G. L. Klimchitskaya, U. Mohideen, and V. M. Mostepanenko, *Advances in the Casimir effect*, Vol. 145 (OUP Oxford, 2009).
- [35] M. Germann, S. Patra, J.-P. Karr, L. Hilico, V. I. Korobov, E. J. Salumbides, K. S. E. Eikema, W. Ubachs, and J. C. J. Koelemeij, Three-body QED test and fifth-force constraint from vibrations and rotations of $\{\text{HD}\}^+$, *Phys. Rev. Research* **3**, L022028 (2021).
- [36] E. J. Salumbides, J. C. J. Koelemeij, J. Komasa, K. Pachucki, K. S. E. Eikema, and W. Ubachs, Bounds on fifth forces from precision measurements on molecules, *Phys. Rev. D* **87**, 112008 (2013).
- [37] M. Jaffe, P. Haslinger, V. Xu, P. Hamilton, A. Upadhye, B. Elder, J. Khoury, and H. Müller, Testing sub-gravitational forces on atoms from a miniature in-vacuum source mass, *Nat Phys* **13**, 938 (2017).
- [38] J. Biesheuvel, J.-P. Karr, L. Hilico, K. S. E. Eikema, W. Ubachs, and J. C. J. Koelemeij, Probing QED and fundamental constants through laser spectroscopy of vibrational transitions in HD^+ , *Nat Commun* **7**, 10385 (2016).
- [39] E. Kahl and J. Berengut, AMBiT: A programme for high-precision relativistic atomic structure calculations, *Computer Physics Communications* **238**, 232 (2019).
- [40] M. A. Levine, R. E. Marrs, J. R. Henderson, D. A. Knapp, and M. B. Schneider, The Electron Beam Ion Trap: A New Instrument for Atomic Physics Measurements, *Physica Scripta* **1988**, 157 (1988).
- [41] M. A. Levine, R. E. Marrs, J. N. Bardsley, P. Beiersdorfer, C. L. Bennett, M. H. Chen, T. Cowan, D. Dietrich, J. R. Henderson, D. A. Knapp, A. Osterheld, B. M. Penetrante, M. B. Schneider, and J. H. Scofield, The use of an electron beam ion trap in the study of highly charged ions, *Nuclear Instruments and Methods in Physics Research Section B: Beam Interactions with Materials and Atoms* **43**, 431 (1989).
- [42] J. R. Crespo López-Urrutia, A. Dorn, R. Moshhammer, and J. Ullrich, The freiburg electron beam ion trap/source project FreEBIT, *Physica Scripta* **T80**, 502 (1999).
- [43] I. Draganić, J. R. Crespo López-Urrutia, R. DuBois, S. Fritzsche, V. M. Shabaev, R. S. Orts, I. I. Tupitsyn, Y. Zou, and J. Ullrich, High precision wavelength measurements of QED-sensitive forbidden transitions in highly charged argon ions, *Phys. Rev. Lett.* **91**, 183001 (2003).
- [44] R. S. Orts, Z. Harman, J. R. C. López-Urrutia, A. N. Artemyev, H. Bruhns, A. J. G. Martínez, U. D. Jentschura, C. H. Keitel, A. Lapierre, V. Mironov, V. M. Shabaev, H. Tawara, I. I. Tupitsyn, J. Ullrich, and A. V. Volotka, Exploring relativistic many-body recoil effects in highly charged ions, *Phys. Rev. Lett.* **97**, 103002 (2006).
- [45] H. Bekker, C. Hensel, A. Daniel, A. Windberger, T. Pfeifer, and J. R. Crespo López-Urrutia, Laboratory precision measurements of optical emissions from coronal iron, *Phys. Rev. A* **98**, 062514 (2018).
- [46] H. Bekker, A. Borschevsky, Z. Harman, C. H. Keitel, T. Pfeifer, P. O. Schmidt, J. R. Crespo López-Urrutia, and J. C. Berengut, Detection of the $5p - 4f$ orbital crossing and its optical clock transition in Pr^{9+} , *Nature Com-*

- munications **10**, 5651 (2019).
- [47] N.-H. Rehbehn, M. K. Rosner, H. Bekker, J. C. Berengut, P. O. Schmidt, S. A. King, P. Micke, M. F. Gu, R. Müller, A. Surzhykov, and J. R. C. López-Urrutia, Sensitivity to new physics of isotope-shift studies using the coronal lines of highly charged calcium ions, *Phys. Rev. A* **103**, L040801 (2021).
- [48] M. F. Gu, The flexible atomic code, *Canadian Journal of Physics* **86**, 675 (2008).
- [49] J. R. Crespo López-Urrutia, P. Beiersdorfer, K. Widmann, and V. Decaux, Visible spectrum of highly charged ions: the forbidden optical lines of Kr, Xe, and Ba ions in the Ar I to Ni I isoelectronic sequence, *Physica Scripta* **T80**, 448 (1999).
- [50] Commission on Isotopic Abundances and Atomic Weights (CIAAW), *Atomic weight of xenon* (2003), (accessed: 2021-08-15).
- [51] S. O. Allehabi, V. A. Dzuba, V. V. Flambaum, A. V. Afanasjev, and S. E. Agbemava, Using isotope shift for testing nuclear theory: The case of nobelium isotopes, *Phys. Rev. C* **102**, 024326 (2020).
- [52] B. J. Bloom, T. L. Nicholson, J. R. Williams, S. L. Campbell, M. Bishof, X. Zhang, W. Zhang, S. L. Bromley, and J. Ye, An optical lattice clock with accuracy and stability at the 10^{-18} level, *Nature* **506**, 71 (2014).
- [53] A. Cingöz, D. C. Yost, T. K. Allison, A. Ruehl, M. E. Fermann, I. Hartl, and J. Ye, Direct frequency comb spectroscopy in the extreme ultraviolet, *Nature* **482**, 68 (2012).
- [54] C. Lyu, S. M. Cavaletto, C. H. Keitel, and Z. Harman, Interrogating the temporal coherence of EUV frequency combs with highly charged ions, *Phys. Rev. Lett.* **125**, 093201 (2020).
- [55] J. Nauta, A. Borodin, H. B. Ledwa, J. Stark, M. Schwarz, L. Schmöger, P. Micke, J. R. Crespo López-Urrutia, and T. Pfeifer, Towards precision measurements on highly charged ions using a high harmonic generation frequency comb, *Nuclear Instruments and Methods in Physics Research Section B: Beam Interactions with Materials and Atoms* **408**, 285 (2017), proceedings of the 18th International Conference on the Physics of Highly Charged Ions (HCI-2016), Kielce, Poland, 11-16 September 2016.
- [56] J. Nauta, J.-H. Oelmann, A. Borodin, A. Ackermann, P. Knauer, I. S. Muhammad, R. Pappenberger, T. Pfeifer, and J. R. C. López-Urrutia, XUV frequency comb production with an astigmatism-compensated enhancement cavity, *Opt. Express* **29**, 2624 (2021).
- [57] S. Weyers, V. Gerginov, M. Kazda, J. Rahm, B. Lipphardt, G. Dobrev, and K. Gibble, Advances in the accuracy, stability, and reliability of the PTB primary fountain clocks, *Metrologia* **55**, 789 (2018).
- [58] J. Guéna, S. Weyers, M. Abgrall, C. Grebing, V. Gerginov, P. Rosenbusch, S. Bize, B. Lipphardt, H. Denker, N. Quintin, S. M. F. Raupach, D. Nicolodi, F. Stefani, N. Chiodo, S. Koke, A. Kuhl, F. Wiotte, F. Meynadier, E. Camisard, C. Chardonnet, Y. L. Coq, M. Lours, G. Santarelli, A. Amy-Klein, R. L. Targat, O. Lopez, P. E. Pottie, and G. Grosche, First international comparison of fountain primary frequency standards via a long distance optical fiber link, *Metrologia* **54**, 348 (2017).
- [59] T. Rosenband, D. B. Hume, P. O. Schmidt, C. W. Chou, A. Brusch, L. Lorini, W. H. Oskay, R. E. Drullinger, T. M. Fortier, J. E. Stalnaker, S. A. Diddams, W. C. Swann, N. R. Newbury, W. M. Itano, D. J. Wineland, and J. C. Bergquist, Frequency ratio of Al⁺ and Hg⁺ single-ion optical clocks; metrology at the 17th decimal place, *Science* **319**, 1808 (2008).
- [60] R. M. Godun, P. B. R. Nisbet-Jones, J. M. Jones, S. A. King, L. A. M. Johnson, H. S. Margolis, K. Szymaniec, S. N. Lea, K. Bongs, and P. Gill, Frequency ratio of two optical clock transitions in ¹⁷¹Yb⁺ and constraints on the time variation of fundamental constants, *Phys. Rev. Lett.* **113**, 210801 (2014).
- [61] K. Beloy, M. I. Bodine, T. Bothwell, S. M. Brewer, S. L. Bromley, J.-S. Chen, J.-D. Deschênes, S. A. Diddams, R. J. Fasano, T. M. Fortier, Y. S. Hassan, D. B. Hume, D. Kedar, C. J. Kennedy, I. Khader, A. Koepke, D. R. Leibrandt, H. Leopardi, A. D. Ludlow, W. F. McGrew, W. R. Milner, N. R. Newbury, D. Nicolodi, E. Oelker, T. E. Parker, J. M. Robinson, S. Romisch, S. A. Schäffer, J. A. Sherman, L. C. Sinclair, L. Sonderhouse, W. C. Swann, J. Yao, J. Ye, X. Zhang, and Boulder Atomic Clock Optical Network (BACON) Collaboration, Frequency ratio measurements at 18-digit accuracy using an optical clock network, *Nature* **591**, 564 (2021).
- [62] T. Manovitz, R. Shaniv, Y. Shapira, R. Ozeri, and N. Akerman, Precision measurement of atomic isotope shifts using a two-isotope entangled state, *Phys. Rev. Lett.* **123**, 203001 (2019).
- [63] Zyriliou, A., Mertzimekis, T. J., Chalil, A., Vasileiou, P., Mavrommatis, E., Bonatsos, Dennis, Martinou, Andriana, Peroulis, S., and Minkov, N., A study of some aspects of the nuclear structure in the even-even Yb isotopes, *Eur. Phys. J. Plus* **137**, 352 (2022).

Supplemental Materials to: Narrow and ultra-narrow transitions in highly charged Xe ions as probes of fifth forces

Nils-Holger Rehbein ¹, Michael K. Rosner ¹, Julian C. Berengut ^{2,1}, Piet O. Schmidt ^{3,4}, Thomas Pfeifer ¹, Ming Feng Gu,⁵ and José R. Crespo López-Urrutia ¹

¹Max-Planck-Institut für Kernphysik, D-69117 Heidelberg, Germany

²School of Physics, University of New South Wales, Sydney, New South Wales 2052, Australia

³Physikalisch-Technische Bundesanstalt, D-38116 Braunschweig, Germany

⁴Leibniz Universität Hannover, D-30167 Hannover, Germany

⁵Space Science Laboratory, University of California, Berkeley, CA 94720, USA

(Dated: October 2, 2023)

I. OTHER SENSITIVE EXCLUSION PAIRS

As the no-mass generalized King plot (GKP) in Fig. ?? we only showed two possible pairs of transitions. Here, we wanted to mention other highly sensitive pairs. Fig. A1 summarizes the transition pairs that yield the best possible sensitivity to a hypothetical fifth-force in the GKP. The order of the pairs do not matter, as the nonlinearity (NL) is the same. The pairs (g, h, i, p) and (a, g, m, o) were the ones shown in Fig. ?. A listing of these transition-pairs can be found in Table B1, where the found lower limit of the coupling constant $y_e y_n$ is given for two mediator masses. Some of these pairs favor a light mediator mass, while others are more sensitive in the keV range. We separated those in the figure and in the table. Other pairings were less sensitive and are omitted.

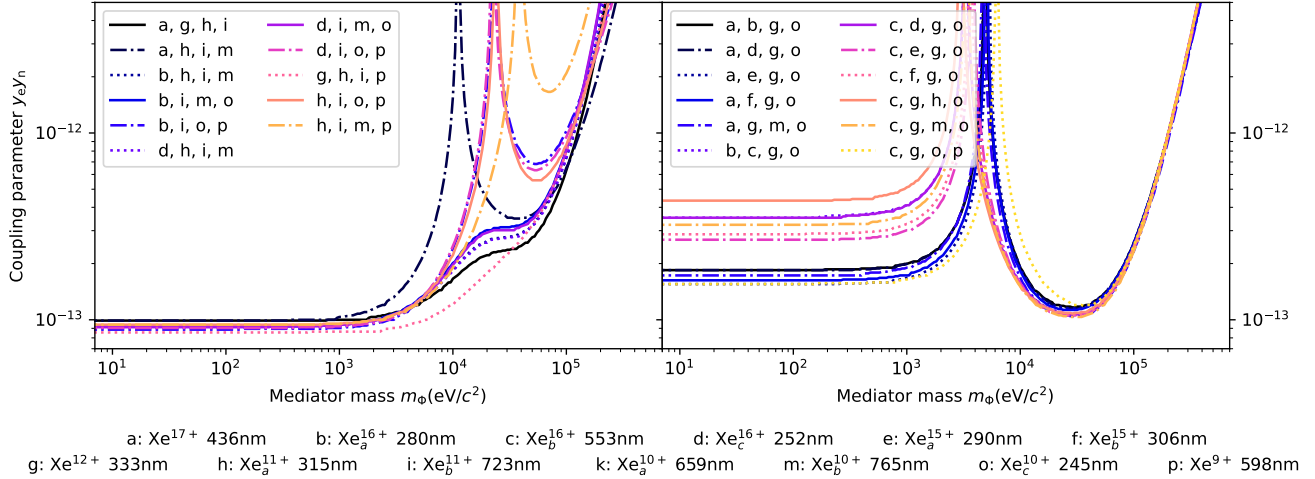


FIG. A1. Lower limit to the coupling constant for different transition pairs to use in the no-mass generalized King plot yielding highest sensitivity. The letters indicate the transition, which can be found at the bottom of the figure.

TABLE B1. List of the exclusion lines from Fig. A1 with their corresponding lower limit of the coupling constant $y_e y_n$ for which the GKP method would be sensitive including current mass uncertainties.

Indices	Transition pairing Transitions	$y_e y_n (m_\Phi)$	
		$m_\Phi = 1 \text{ eV}/c^2$	$m_\Phi = 30 \text{ keV}/c^2$
a g h i	Xe ¹⁷⁺ (436 nm), Xe ¹²⁺ (333 nm), Xe ¹¹⁺ (315 nm), Xe ¹¹⁺ (723 nm)	9.9×10^{-14}	2.37×10^{-13}
a h i m	Xe ¹⁷⁺ (436 nm), Xe ¹¹⁺ (315 nm), Xe ¹¹⁺ (723 nm), Xe ¹⁰⁺ (765 nm)	9.9×10^{-14}	3.52×10^{-13}
b h i m	Xe ¹⁶⁺ (280 nm), Xe ¹¹⁺ (315 nm), Xe ¹¹⁺ (723 nm), Xe ¹⁰⁺ (765 nm)	9.1×10^{-14}	2.79×10^{-13}
b i o m	Xe ¹⁶⁺ (280 nm), Xe ¹¹⁺ (723 nm), Xe ¹⁰⁺ (765 nm), Xe ¹⁰⁺ (245 nm)	9.2×10^{-14}	3.13×10^{-13}
b i o p	Xe ¹⁶⁺ (280 nm), Xe ¹¹⁺ (723 nm), Xe ¹⁰⁺ (245 nm), Xe ⁹⁺ (598 nm)	8.8×10^{-14}	12.96×10^{-13}
d h i m	Xe ¹⁶⁺ (252 nm), Xe ¹¹⁺ (315 nm), Xe ¹¹⁺ (723 nm), Xe ¹⁰⁺ (765 nm)	9.1×10^{-14}	2.74×10^{-13}
d i o m	Xe ¹⁶⁺ (252 nm), Xe ¹¹⁺ (723 nm), Xe ¹⁰⁺ (765 nm), Xe ¹⁰⁺ (245 nm)	9.1×10^{-14}	3.02×10^{-13}
d i o p	Xe ¹⁶⁺ (252 nm), Xe ¹¹⁺ (723 nm), Xe ¹⁰⁺ (245 nm), Xe ⁹⁺ (598 nm)	9.0×10^{-14}	11.41×10^{-13}
g h i p	Xe ¹²⁺ (333 nm), Xe ¹¹⁺ (315 nm), Xe ¹¹⁺ (723 nm), Xe ⁹⁺ (598 nm)	8.6×10^{-14}	2.21×10^{-13}
h i o p	Xe ¹¹⁺ (315 nm), Xe ¹¹⁺ (723 nm), Xe ¹⁰⁺ (245 nm), Xe ⁹⁺ (598 nm)	9.4×10^{-14}	11.88×10^{-13}
h i m p	Xe ¹¹⁺ (315 nm), Xe ¹¹⁺ (723 nm), Xe ¹⁰⁺ (765 nm), Xe ⁹⁺ (598 nm)	9.4×10^{-14}	16.33×10^{-13}
a b g o	Xe ¹⁷⁺ (436 nm), Xe ¹⁶⁺ (280 nm), Xe ¹²⁺ (333 nm), Xe ¹⁰⁺ (245 nm)	18.4×10^{-14}	1.16×10^{-13}
a d g o	Xe ¹⁷⁺ (436 nm), Xe ¹⁶⁺ (252 nm), Xe ¹²⁺ (333 nm), Xe ¹⁰⁺ (245 nm)	18.4×10^{-14}	1.15×10^{-13}
a e g o	Xe ¹⁷⁺ (436 nm), Xe ¹⁵⁺ (290 nm), Xe ¹²⁺ (333 nm), Xe ¹⁰⁺ (245 nm)	15.5×10^{-14}	1.15×10^{-13}
a f g o	Xe ¹⁷⁺ (436 nm), Xe ¹⁵⁺ (306 nm), Xe ¹²⁺ (333 nm), Xe ¹⁰⁺ (245 nm)	16.3×10^{-14}	1.13×10^{-13}
a g m o	Xe ¹⁷⁺ (436 nm), Xe ¹²⁺ (333 nm), Xe ¹⁰⁺ (765 nm), Xe ¹⁰⁺ (245 nm)	17.3×10^{-14}	1.05×10^{-13}
b c g o	Xe ¹⁶⁺ (280 nm), Xe ¹⁶⁺ (553 nm), Xe ¹²⁺ (333 nm), Xe ¹⁰⁺ (245 nm)	35.2×10^{-14}	1.08×10^{-13}
c d g o	Xe ¹⁶⁺ (553 nm), Xe ¹⁶⁺ (252 nm), Xe ¹²⁺ (333 nm), Xe ¹⁰⁺ (245 nm)	35.2×10^{-14}	1.07×10^{-13}
c e g o	Xe ¹⁶⁺ (553 nm), Xe ¹⁵⁺ (290 nm), Xe ¹²⁺ (333 nm), Xe ¹⁰⁺ (245 nm)	26.8×10^{-14}	1.06×10^{-13}
c f g o	Xe ¹⁶⁺ (553 nm), Xe ¹⁵⁺ (306 nm), Xe ¹²⁺ (333 nm), Xe ¹⁰⁺ (245 nm)	28.7×10^{-14}	1.06×10^{-13}
c g h o	Xe ¹⁶⁺ (553 nm), Xe ¹²⁺ (333 nm), Xe ¹¹⁺ (315 nm), Xe ¹⁰⁺ (245 nm)	43.4×10^{-14}	1.09×10^{-13}
c g m o	Xe ¹⁶⁺ (553 nm), Xe ¹²⁺ (333 nm), Xe ¹⁰⁺ (765 nm), Xe ¹⁰⁺ (245 nm)	32.3×10^{-14}	1.04×10^{-13}
c g o p	Xe ¹⁶⁺ (553 nm), Xe ¹²⁺ (333 nm), Xe ¹⁰⁺ (245 nm), Xe ⁹⁺ (598 nm)	15.5×10^{-14}	1.20×10^{-13}

II. GROTRIAN DIAGRAMS AND OTHER IDENTIFIED TRANSITIONS

To summarize the identified transitions, besides the ones involving the ground-level, and to allow an insight about potentially interesting transitions, Grotrian diagrams are listed in Fig. A2. Xe¹⁰⁺ has one E2 transition without an energy level in-between the upper and lower level, which can be found by calculating with the identified transitions. Xe¹²⁺ exhibits two potentially interesting E2 transitions, but further measurements are necessary to determine them and what energy the intermediate levels have. Their theoretically expected transitions and transition rates are added based on calculations by AMBIT.

TABLE B2. Other identified transitions in Xe¹⁰⁺. An E2 and a M1 transition were calculated based on identified transitions via Rydberg-Ritz combinations. Transition details, ab-initio wavelength λ_{ambit} and A_{ki} values based on AMBIT calculations.

Ion	Transition	Energy (eV)	λ_{vac} (nm)	λ_{ambit} (nm)	A_{ki} (s ⁻¹)	Type	Note
Xe ¹⁰⁺	$4d^8 \ ^1D_2 - \ ^3F_3$	3.4276528(10)	361.71748(10)	353.6	159.5	M1	
Xe ¹⁰⁺	$4d^8 \ ^1G_4 - \ ^3F_3$	3.1758602(72)	390.39563(88)	382.6	10.7	M1	
Xe ¹⁰⁺	$4d^8 \ ^3P_1 - \ ^3F_2$	2.6655150(26)	465.14163(45)	453.7	47.8	M1	
Xe ¹⁰⁺	$4d^8 \ ^1D_2 - \ ^3P_2$	2.0067271(28)	617.84283(85)	615.9	55.8	M1	
Xe ¹⁰⁺	$4d^8 \ ^3P_2 - \ ^3F_2$	1.68081600(90)	737.64289(39)	741.4	35.3	M1	
Xe ¹⁰⁺	$4d^8 \ ^1G_4 - \ ^3F_4$	5.0567231(73)	245.18684(36)	242.9	67.1	M1	obtained by Ritz-Rydberg combination
Xe ¹⁰⁺	$4d^8 \ ^3F_2 - \ ^3F_4$	1.6209726(34)	764.8753(16)	735.6	0.002	E2	obtained by Ritz-Rydberg combination

Table B3 lists the transitions from Fig. A2 with their measured vacuum wavelength λ_{vac} and energy, as well as AMBIT ab-initio wavelengths and A_{ki} values. Ground-level transitions from Table ?? are not listed. Ambiguous identifications are noted as preliminary and supplemental measurements would be needed. Interesting electric quadrupole E2 transitions were pointed out by noting them as AMBIT results. Where Rydberg-Ritz combination allowed identification, those were noted as such.

Xe¹⁰⁺ has been separated to Table B2, where an E2 transition was identified via Rydberg-Ritz combination. This clock transition has a lifetime of around 500s, thus a natural line-width of 0.3 mHz.

While Xe¹²⁺ has two possible E2 transitions, no connection between measured lines was found and further inves-

TABLE B3. Identified transitions in xenon, besides the ground-level transitions. Some interesting E2 transitions were calculated based on identified transitions. Some were added solely based on ab-initio AMBIT calculations, to point them out. Lines with a preliminary note did not convey enough information to be identified without ambiguity, e.g., Zeeman structure was not sufficiently resolved or too many lines were too close to each other. Transition details, ab-initio wavelength λ_{ambit} and A_{ki} values are based on AMBIT calculations.

Ion	Transition	Energy (eV)	λ_{vac} (nm)	λ_{ambit} (nm)	A_{ki} (s^{-1})	Type	Note
Xe ¹¹⁺	$4d^7 \ ^2D_{5/2} - \ ^4F_{7/2}$	4.397932(52)	281.9147(33)	272.9	246.1	M1	
Xe ¹¹⁺	$4d^7 \ ^2H_{9/2} - \ ^2G_{9/2}$	3.1523(48)	393.3(6)	395.9	99.6	M1	
Xe ¹¹⁺	$4d^7 \ ^2D_{5/2} - \ ^4P_{3/2}$	2.8739(33)	431.42(49)	422.0	42.4	M1	
Xe ¹¹⁺	$4d^7 \ ^2D_{3/2} - \ ^4P_{3/2}$	2.5866(22)	477.713(90)	468.0	104.4	M1	
Xe ¹¹⁺	$4d^7 \ ^4P_{3/2} - \ ^4P_{3/2}$	2.5707010(33)	482.29723(62)	474.9	113.5	M1	
Xe ¹¹⁺	$4d^7 \ ^2D_{5/2} - \ ^4P_{5/2}$	2.4899(15)	497.93(29)	494.9	27.4	M1	
Xe ¹¹⁺	$4d^7 \ ^2D_{3/2} - \ ^2D_{5/2}$	2.29265(30)	540.790(70)	533.8	53.9	M1	
Xe ¹¹⁺	$4d^7 \ ^2G_{9/2} - \ ^4F_{7/2}$	2.21997(16)	558.50(4)	550.3	8.8	M1	
Xe ¹¹⁺	$4d^7 \ ^4P_{3/2} - \ ^4P_{5/2}$	2.18799(39)	566.66(10)	569.2	61.8	M1	
Xe ¹¹⁺	$4d^7 \ ^2P_{5/2} - \ ^4F_{7/2}$	1.907216(88)	650.079(30)	608.4	16.7	M1	
Xe ¹¹⁺	$4d^7 \ ^2F_{7/2} - \ ^2G_{7/2}$	3.0825(38)	402.21(50)	361.5	37.7	M1	preliminary
Xe ¹¹⁺	$4d^7 \ ^2F_{5/2} - \ ^2G_{7/2}$	2.5732(21)	481.83(39)	525.0	6.7	M1	preliminary
Xe ¹¹⁺	$4d^7 \ ^2P_{1/2} - \ ^4P_{1/2}$	2.42089(80)	512.14(16)	510.7	129.1	M1	preliminary
Xe ¹¹⁺	$4d^7 \ ^4P_{1/2} - \ ^4F_{3/2}$	2.03614(13)	608.918(40)	597.5	21.5	M1	preliminary
Xe ¹¹⁺	$4d^7 \ ^2H_{9/2} - \ ^2H_{11/2}$	1.842646(25)	672.860(9)	674.3	29.3	M1	preliminary
Xe ¹¹⁺	$4d^7 \ ^2D_{3/2} - \ ^2P_{1/2}$	1.76973(23)	700.583(90)	732.5	10.1	M1	preliminary
Xe ¹¹⁺	$4d^7 \ ^4P_{5/2} - \ ^4F_{5/2}$	1.54551(39)	802.22(20)	837.6	5.8	M1	preliminary
Xe ¹²⁺	$4d^6 \ ^3D_1 - \ ^3P_2$	3.7282435(96)	332.55391(86)	340.1	105.5	M1	
Xe ¹²⁺	$4d^6 \ ^3P_2 - \ ^5D_3$	3.278867(10)	378.1313(12)	365.2	203.9	M1	
Xe ¹²⁺	$4d^6 \ ^1I_6 - \ ^3H_6$	3.327889(18)	372.5611(20)	373.2	72.4	M1	preliminary
Xe ¹²⁺	$4d^6 \ ^1G_4 - \ ^3H_4$	3.0372(30)	408.21(39)	394.5	121.3	M1	preliminary
Xe ¹²⁺	$4d^6 \ ^3P_2 - \ ^5D_1$	2.81415(10)	440.57(15)	459.0	66.0	M1	preliminary
Xe ¹²⁺	$4d^6 \ ^3F_2 - \ ^1F_3$	2.4539(11)	505.25(22)	480.6	63.6	M1	preliminary
Xe ¹²⁺	$4d^6 \ ^3G_4 - \ ^3H_5$	2.42449(90)	511.38(18)	505.6	33.8	M1	preliminary
Xe ¹²⁺	$4d^6 \ ^3H_4 - \ ^3H_4$	2.36708(45)	523.79(10)	527.9	120.3	M1	preliminary
Xe ¹²⁺	$4d^6 \ ^3G_5 - \ ^3H_6$	2.2546375(23)	549.90744(55)	540.0	54.3	M1	preliminary
Xe ¹²⁺	$4d^6 \ ^3D_1 - \ ^3P_2$	2.23393(12)	555.01(3)	549.9	75.9	M1	preliminary
Xe ¹²⁺	$4d^6 \ ^3P_2 - \ ^3P_1$	2.19676(47)	564.39(11)	584.9	60.8	M1	preliminary
Xe ¹²⁺	$4d^6 \ ^3P_1 - \ ^3P_0$	2.17953(38)	568.86(10)	592.8	54.6	M1	preliminary
Xe ¹²⁺	$4d^6 \ ^3D_3 - \ ^3F_2$	1.928492(90)	642.907(30)	636.9	31.6	M1	preliminary
Xe ¹²⁺	$4d^6 \ ^5D_2 - \ ^5D_4$	1.3306		931.8	7.2×10^{-4}	E2	AMBIT result
Xe ¹²⁺	$4d^6 \ ^3H_6 - \ ^5D_4$	4.5152		274.6	9.6×10^{-5}	E2	AMBIT result
Xe ¹⁵⁺	$4d^3 \ ^2G_{9/2} - \ ^2G_{7/2}$	3.2906036(29)	376.78253(33)	376.7	162.6	M1	
Xe ¹⁵⁺	$4d^3 \ ^4P_{3/2} - \ ^4P_{3/2}$	3.1088401(49)	398.81175(62)	397.9	198.8	M1	
Xe ¹⁵⁺	$4d^3 \ ^2H_{9/2} - \ ^4F_{7/2}$	3.096290(15)	400.428(2)	394.2	76.5	M1	
Xe ¹⁵⁺	$4d^3 \ ^2G_{9/2} - \ ^2H_{9/2}$	3.056024(16)	405.7042(21)	400.6	160.5	M1	
Xe ¹⁵⁺	$4d^3 \ ^2G_{7/2} - \ ^4F_{7/2}$	2.861683(14)	433.2561(21)	420.4	65.7	M1	
Xe ¹⁵⁺	$4d^3 \ ^2D_{5/2} - \ ^4P_{5/2}$	2.41424(85)	513.55(17)	501.1	11.8	M1	
Xe ¹⁵⁺	$4d^3 \ ^2H_{9/2} - \ ^4F_{9/2}$	2.286319(11)	542.2875(25)	536.6	82.9	M1	
Xe ¹⁵⁺	$4d^3 \ ^4P_{5/2} - \ ^4P_{3/2}$	2.2483297(50)	551.4502(12)	554.1	59.6	M1	
Xe ¹⁵⁺	$4d^3 \ ^2D_{5/2} - \ ^3P_{3/2}$	1.55279(97)	798.45(49)	777.0	18.1	M1	
Xe ¹⁵⁺	$4d^3 \ ^2F_{7/2} - \ ^2G_{7/2}$	4.269411(14)	290.40114(96)	278.6	50.6	M1	preliminary
Xe ¹⁵⁺	$4d^3 \ ^2P_{1/2} - \ ^4P_{1/2}$	3.123792(52)	396.9028(66)	392.8	233.2	M1	preliminary
Xe ¹⁵⁺	$4d^3 \ ^4P_{3/2} - \ ^4F_{5/2}$	2.06849(17)	599.395(50)	548.0	10.3	M1	preliminary
Xe ¹⁵⁺	$4d^3 \ ^2H_{11/2} - \ ^2H_{9/2}$	1.988448(64)	623.522(20)	615.4	30.3	M1	preliminary
Xe ¹⁶⁺	$4d^2 \ ^1G_4 - \ ^3F_4$	3.14220(18)	394.577(22)	383.2	69.5	M1	
Xe ¹⁶⁺	$4d^2 \ ^3P_2 - \ ^1D_2$	3.0230061(48)	410.13545(65)	407.7	165.2	M1	
Xe ¹⁶⁺	$4d^2 \ ^3P_2 - \ ^3P_1$	2.5194098(20)	492.11604(39)	489.0	61.2	M1	
Xe ¹⁶⁺	$4d^2 \ ^1D_2 - \ ^3F_3$	2.17991(38)	568.8(1)	530.3	20.2	M1	
Xe ¹⁶⁺	$4d^2 \ ^3F_4 - \ ^3F_3$	1.7426542(51)	711.4675(21)	701.8	50.6	M1	
Xe ¹⁶⁺	$4d^2 \ ^3P_1 - \ ^3F_2$	4.9243614(65)	251.77721(33)	244.3	10.3	M1	obtained by Ritz-Rydberg combination
Xe ¹⁶⁺	$4d^2 \ ^3P_0 - \ ^3F_2$	3.7766		328.2	1.05	E2	AMBIT result